Strain Ultrasound Elastography of Aneurysm Sac Content after Randomized Endoleak Embolization with Sclerosing vs. Non-sclerosing Chitosan-based Hydrogels in a Canine Model

Lojan Sivakumaran, MDCM, MSc, Husain Alturkistani, MD, Sophie Lerouge, PhD, Antony Bertrand-Grenier, PhD, Fatemeh Zehtabi, PhD, Éric Thérasse, MD, Marie-Hélène Roy-Cardinal, PhD, Sahir Bhatnagar, PhD, Guy Cloutier, PhD, and Gilles Soulez, MD, MSc

ABSTRACT

Purpose: To compare the mechanical properties of aneurysm content after endoleak embolization with a chitosan hydrogel (CH) with that with a chitosan hydrogel with sodium tetradecyl sulfate (CH-STS) using strain ultrasound elastography (SUE).

Materials and Methods: Bilateral common iliac artery type Ia endoleaks were created in 9 dogs. Per animal, 1 endoleak was randomized to blinded embolization with CH, and the other, with CH-STS. Brightness-mode ultrasound, Doppler ultrasound, SUE radiofrequency ultrasound, and computed tomography were performed for up to 6 months until sacrifice. Radiologic and histopathologic studies were coregistered to identify 3 regions of interest: the embolic agent, intraluminal thrombus (ILT), and aneurysm sac. SUE segmentations were performed by 2 blinded independent observers. The maximum axial strain (MAS) was the primary outcome. Statistical analysis was performed using the Fisher exact test, multivariable linear mixed-effects models, and intraclass correlation coefficients (ICCs).

Results: Residual endoleaks were identified in 7 of 9 (78%) and 4 of 9 (44%) aneurysms embolized with CH and CH-STS, respectively (P = .3348). CH-STS had a 66% lower MAS (P < .001) than CH. The ILT had a 37% lower MAS (P = .01) than CH and a 77% greater MAS (P = .079) than CH-STS. There was no significant difference in ILT between treatments. The aneurysm sacs embolized with CH-STS had a 29% lower MAS (P < .001) than those embolized with CH. Residual endoleak was associated with a 53% greater MAS (P < .001). The ICC for MAS was 0.807 (95% confidence interval: 0.754–0.849) between segmentations.

Conclusions: CH-STS confers stiffer intraluminal properties to embolized aneurysms. Persistent endoleaks are associated with increased sac strain, an observation that may help guide management.

ABBREVIATIONS

AAA = abdominal aortic aneurysm, B-mode = brightness mode, CH = chitosan hydrogel, CI = confidence interval, CT = computed tomography, ICC = intraclass correlation coefficient, ILT = intraluminal thrombus, MAS = maximum axial strain, ROI = region of interest, STS = sodium tetradecyl sulfate, SUE = strain ultrasound elastography

Endoleaks are a therapeutic challenge. The failure of endoleak embolization (usually of type II endoleaks) occurs in half of cases and may be secondary to the persistence of the endothelial layer (1,2). Recently, an embolic agent containing a biocompatible radiopaque chitosan hydrogel (CH) and the sclerosant sodium tetradecyl sulfate (STS) was developed to promote vascular occlusion and endothelial ablation (3,4). Named CH-STS, the agent has shown

RESEARCH HIGHLIGHTS

- The mechanical properties of aneurysm content after endoleak embolization were characterized using strain ultrasound elastography, comparing 2 new embolic agents: chitosan hydrogel (CH) versus chitosan hydrogen with the sclerosant sodium tetradecyl sulfate (CH-STS).

- The CH-STS agent demonstrated a 66% lower strain ($P < .001$) in vivo than the CH agent.

- The aneurysm sac content of endoleaks embolized with CH-STS showed a 29% lower strain ($P < .001$) than endoleaks embolized with CH, independent of the presence of residual endoleak.

- Endoleak persistence was associated with a 53% greater strain of the aneurysm sac content ($P < .001$), independent of the embolic agent used.

favorable in vitro mechanical properties—with respect to gelation time, storage modulus, and occlusivity—and a superior ability to denude the endothelium compared with a similar, nonsclerosing agent (CH) (3,4). The agents' in vivo behavior, however, merits further characterization.

Strain ultrasound elastography (SUE) is an emerging ultrasound-based technique that is well suited to assess the mechanical properties of embolic agents. SUE calculates tissue strain—or relative change in dimension—using changes in ultrasound-derived radiofrequency signals before and after the application of a force, such as from cardiovascular pulsations (5,6). The greater the change in the dimension of an imaged structure (with a given force), the lower is its stiffness. Previously, SUE has been used to identify endoleaks and to differentiate organized and fresh thrombi in abdominal aortic aneurysm (AAA) and endoleak models (7,8).

The strain analysis of AAA intraluminal content may also provide important prognostic information. Lower AAA content stiffness is associated with aneurysm nonshrinkage/expansion, greater aneurysm wall stress, and rupture (via direct transmission of arterial pressure to the vessel wall) (7–12). Therefore, the confirmation of an embolic agent's ability to decrease intraluminal content strain would not only positively reflect its mechanical occlusivity but also its ability to attenuate wall stress. Furthermore, as previously described, strain analysis may eventually play an adjunctive role in the follow-up of recurrent endoleaks to help guide management (7).

The goal of this study was to characterize the mechanical properties of the embolic agents, intraluminal thrombus (ILT), and aneurysm sac content after endoleak embolization with CH-STS and CH using SUE.

MATERIALS AND METHODS

Protocols were approved by the institutional animal care committee.

Aneurysm and Endoleak Model

Bilateral common iliac artery type Ia endoleaks were constructed in 9 mongrel dogs (25–50 kg), creating a total of 18 endoleaks, according to a previously described technique (**Fig 1**) (2,4,13). A full description of the surgical aneurysm creation, endoleak creation, agent preparation, randomization, and embolization is provided in **Appendix A** (available online on the article's Supplemental Material page at *www.jvir.org*).

Follow-up Imaging and Histopathology

Six animals were followed for 3 months and 3 animals were followed for 6 months before sacrifice in the context of another experiment (4). Nonstrain imaging modalities and histopathology were used to detect endoleaks and to facilitate the segmentation of the regions of interest (ROIs) (described in the following section) for strain imaging. Acquisition parameters and histologic preparations are detailed in **Appendix A** (available online at *www.jvir.org*).

Ultrasound Acquisitions. Brightness-mode (B-mode) images, Doppler ultrasound images, and cine radiofrequency acquisitions for SUE were obtained of the proximal, middle, and distal aneurysm sac at 1 week, 1 month, and 3 months after embolization in all subjects, with an additional 6-month follow-up in 3 subjects.

Computed Tomography. Contrast-enhanced computed tomography (CT) scans were obtained 3 months after embolization in all subjects and at 6 months after embolization in 3 subjects. CT was the gold standard for diagnosing endoleaks.

Tissue Analysis. Animals were sacrificed, and the aneurysms were harvested en bloc and fixed in buffered formalin. Serial axial macroscopic sections were obtained and photographed for a macroscopic analysis. Representative histologic slides were produced with hematoxylin phloxine saffron staining to correlate the macroscopic and microscopic findings. Tissue analysis was supervised by a biomedical engineer with >20 years' experience in biomaterial research (S.L.).

ROIs for SUE

SUE was performed on 3 ROIs: (*a*) the embolic agent at sacrifice, (*b*) the ILT at sacrifice, and (*c*) the aneurysm sac at all time points. **Table E1** (available online at *www.jvir.org*) details the imaging/histopathologic characteristics.
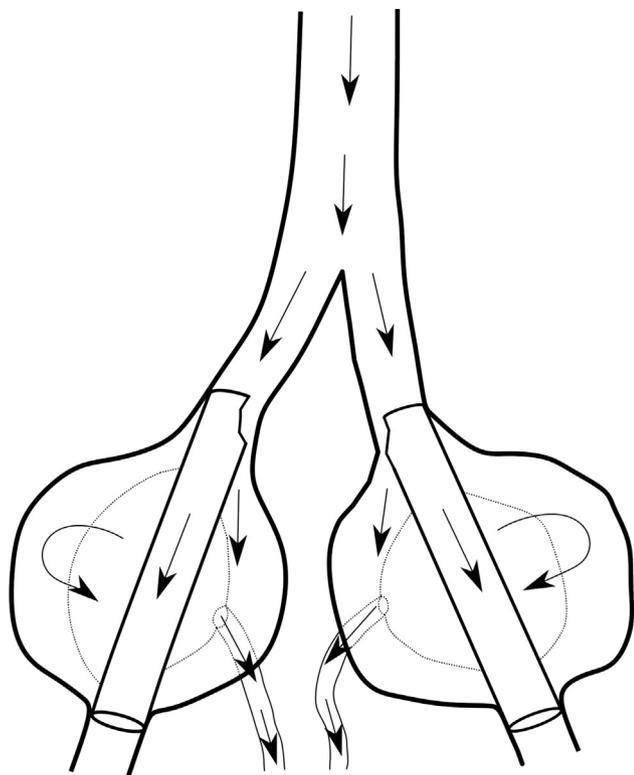
Figure 1. Schematic of the bilateral high-flow type Ia endoleak common iliac aneurysm model for the assessment of the embolic agents. The iliac arteries were surgically incised, anastomosed with transposed sacroiliac trunks, and patched with jugular venous grafts. Endovascular aneurysm repair was performed 8 weeks after the surgery using a balloon-expandable stent graft. The stents were deformed using a balloon along the proximal landing zone to create endoleaks. The arrows indicate the direction of blood flow.

Image Coregistration and Strain Analysis

The cine radiofrequency acquisitions were imported to an imaging platform (ORS Visual; Montreal, Canada) and converted to B-mode cines. Each cine was coregistered with the relevant radiologic and histopathologic studies at all follow-up time points based on the acquisition level, aneurysm morphology, and the relative location position of the stent graft in the aneurysm.

SUE was performed using the radiofrequency cines with a previously described in-house algorithm on ORS Visual (6). Each ROI (aneurysm sac, thrombus, and agent) was manually contoured (ie, drawn) on 1 cine frame by 2 independent readers (a radiology resident (L.S.) and an interventional radiologist with 30 years' experience (G.S.)) with the help of the coregistered modalities; the readers were blinded to the agent used. The contours of each ROI were propagated to the remaining frames of the cine using a validated automatic technique (with an average absolute point-to-point distance of 0.24 mm compared to an expert's manually drawn contours [14]). The SUE algorithm was then used to calculate the time-varying instantaneous and

Table 1. Definition of the Strain and Shear Strain Elastography Parameters Obtained with Strain Ultrasound Elastography using a Lagrangian Speckle Model Estimator

Parameter	Definition
Maximum axial strain (%)	The maximum axial strain is the peak dilation of the segmented tissue during each cardiac cycle, averaged over multiple cardiac cycles.
Range of cumulative axial strain (%)	The range of the cumulative axial strain is the total compression/dilation of the segmented tissue during each cardiac cycle, averaged over multiple cardiac cycles.
Range of cumulative axial shear strain (%)	The range of the cumulative axial strain corresponds to the total angular change of a segmented tissue (from a rectangular shape to parallelogram) during each cardiac cycle, averaged over multiple cardiac cycles.

cumulative axial strain and axial shear strain curves based on the deformation detected within the ROIs (see **Appendix A** [available online at *www.jvir.org*] for further details). After the processing phase, performed by the radiology trainee, the curves were divided into cardiac cycles to generate 3 imaging parameters: the maximum axial strain (MAS), range of cumulative axial strain, and range of cumulative axial shear strain. The strain parameters are defined in **Table 1**.

Statistical Analysis

Statistical analysis was performed using R software (version 3.6.0; R Foundation, Vienna, Austria). The sample size was chosen to detect an approximately 30%–60% difference in the MAS between the CH and CH-STS ROIs (depending on the projected standard deviations). The strain and shear strain values obtained using the segmentations of the senior reader are presented. The Fisher exact test was used to compare the number of residual endoleaks between the treatment groups. Multivariable linear mixed-effects models were used to model the mechanical properties of the agent, ILT, and aneurysm sac ROIs and to compare the mechanical properties of the agent ROIs with those of the ILT. This is justified in **Appendix A** (available online at *www.jvir.org*). Interobserver reliability between the segmentations of the 2 readers was calculated using intraclass correlation coefficients (ICCs) with a 2-way random-effects model for a single measure for consistency. Outcomes were log transformed to produce better model fits. The regression coefficients represent the estimated mean percentage change in the outcome between 2 groups. The level of significance was set at α value of 0.05, and 95% confidence intervals (CIs) were calculated using the profile likelihood.

RESULTS
Baseline Characteristics

Endoleak construction was successful in all animals. At sacrifice, 7 of 9 (78%) and 4 of 9 (44%) aneurysms embolized with CH and CH-STS had residual endoleaks, respectively ($P = .3348$). There was 1 complication of stent
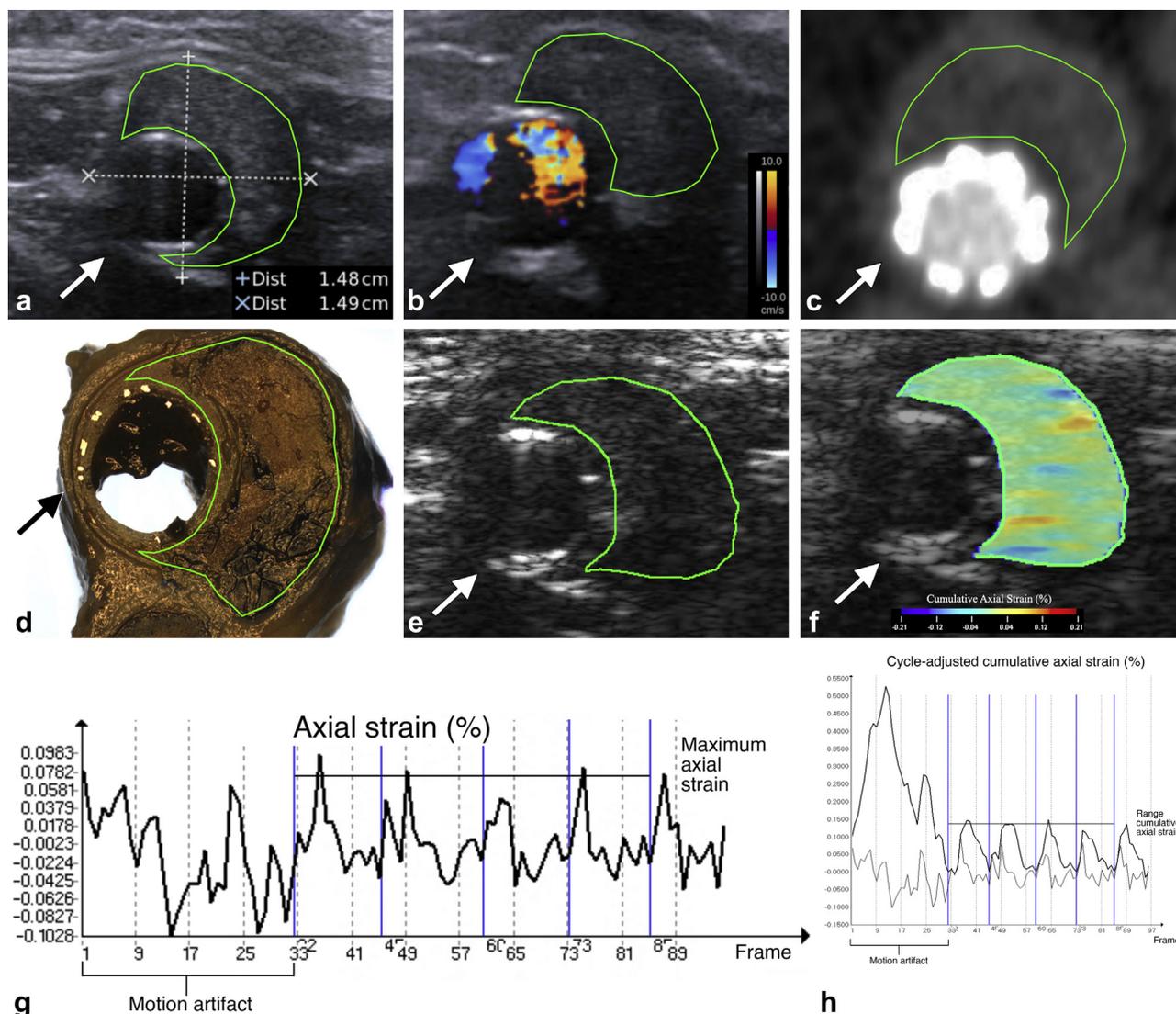
Figure 2. Multimodal image coregistration, segmentation, and postprocessing of the aneurysm sac region of interest (ROI) for an aneurysm 6 months after successful embolization with the chitosan hydrogel with sodium tetradecyl sulfate (CH-STS) at sacrifice. **(a)** Brightness-mode (B-mode) image of the distal level of an aneurysm 6 months after embolization with CH-STS. The aneurysm sac is segmented in green. The arrow indicates the stent graft. The dashed line bounded by +'s represents the anterior-posterior dimension of the aneurysm. The dashed line bounded by x's designates the lateral dimensions of the aneurysm. **(b)** Doppler ultrasound image of the distal level of an aneurysm 6 months after embolization with CH-STS. The aneurysm sac is segmented in green. The arrow indicates the stent graft. There is no endoleak. **(c)** Contrast-enhanced computed tomography image of the distal level of an aneurysm 6 months after embolization with CH-STS. The aneurysm sac is segmented in green. The arrow indicates the stent graft. There is no endoleak. **(d)** A macroscopic section of the distal level of an aneurysm 6 months after embolization with CH-STS. The aneurysm sac is segmented in green. The arrow indicates the stent graft. There is no endoleak. **(e)** A selected B-mode image (from the cine loop used to produce the elastograms) of the distal level of an aneurysm 6 months after embolization with CH-STS. The aneurysm sac is segmented in green. The arrow indicates the stent graft. **(f)** A selected B-mode image (from the cine loop used to produce the elastograms) of the distal level of an aneurysm 6 months after embolization with CH-STS with the overlying cumulative axial strain map. The aneurysm sac is segmented in green. The instantaneous cumulative axial values within the ROI are displaced as a color map within the segmented region. The arrow indicates the stent graft. **(g)** An instantaneous axial strain curve of the aneurysm sac ROI of the distal level of an aneurysm 6 months after embolization with CH-STS. The maximum axial strain parameter (average of all peaks) is labeled. Note that the frames containing the motion artifact (seen on the cine loops) were excluded from the analysis. **(h)** The cycle-adjusted cumulative axial strain curve (thicker curve; the thinner curve is again the axial strain curve) of the aneurysm sac ROI of the distal level of an aneurysm 6 months after embolization with CH-STS. The range of the cumulative axial strain parameter is labeled. Note that the frames containing the motion artifact (seen on the cine loops) were excluded from the analysis.

Table 2. Maximum Axial Strain, Range of Cumulative Axial Strain, and Range of Cumulative Axial Shear Strain of the Embolic Agent Region of Interest at Sacrifice

Embolic agent	Endoleak present	Maximum axial strain (%)	Range of cumulative axial strain (%)	Range of cumulative axial shear strain (%)
CH-STS	Yes (n = 3)	0.111 ± 0.090	0.226 ± 0.098	0.759 ± 0.184
	No (n = 5)	0.088 ± 0.082	0.188 ± 0.127	0.681 ± 0.210
CH	Yes (n = 7)	0.224 ± 0.099	0.535 ± 0.280	0.855 ± 1.044
	No (n = 2)	0.262 ± 0.056	0.691 ± 0.084	1.188 ± 0.934

Note–Values are presented as mean ± standard deviation. "n" indicates the number of aneurysms.
CH = chitosan hydrogel; CH-STS = chitosan hydrogel with sodium tetradecyl sulfate.

graft thrombosis in the CH group with a persistent endoleak; this animal was included in the analysis.

Radiologic studies and tissue correlates were successfully coregistered (Fig 2a–h). All anticipated elastograms were generated with 1 exception: 1 unsuccessful CH-STS embolization had no residual embolic agent remaining in the sac due to a challenging bilobed morphology. Therefore, this ROI could not be segmented. In total, 430 total elastograms were generated, 215 per reader.

Strain Analysis of Embolic Agents

The mechanical properties of the embolic agent ROI are presented in Table 2. The estimated regression coefficients for the final model are presented in Table 3. CH-STS had a 66% lower MAS ($P < .001$) (Fig 3a) and a 67% lower range of the cumulative axial strain ($P < .001$) than CH when considering all cases (both with and without endoleak). The ranges of the cumulative axial shear strains of the embolic agents were not significantly different between the treatment groups.

Strain Analysis of ILT

The mechanical properties of the ILT ROI stratified by the type of embolic agent used and the presence of endoleak are presented in Table 4. The multivariable linear mixed-effects model revealed that neither the type of the agent used nor the presence of endoleak was a significant predictor of the ILT strain or shear strain outcomes (Table 5 and Fig 3b).

Comparison of Embolic Agent and ILT Strain

The ILT was found to have a 37% lower MAS ($P = .01$) and a 37% lower range of the cumulative axial strain ($P = .017$) than CH when comparing all aneurysms embolized with CH. In contrast, the ILT had a 77% greater MAS ($P = .079$, approaching significance) and a 59% greater range of the cumulative axial strain ($P = .047$) than CH-STS when comparing all aneurysms embolized with CH-STS. Therefore, the strain of the ILT was between those of CH and CH-STS, being greater than the former and lesser than the latter. There was no significant difference between the shear strain values of CH or CH-STS compared with the ILT.

Strain Analysis of Aneurysm Sac ROI

The mechanical properties of the aneurysm sac ROIs are presented in Table 6. The estimated regression coefficients of the final model are presented in Table 7. The use of CH-STS was associated with a 29% lower MAS ($P < .001$) (Fig 3c), a 28% lower range of the cumulative axial strain ($P < .001$), and a 27% lower range of the cumulative axial shear strain ($P < .001$) of the aneurysm sac, while controlling for the presence of endoleak. Endoleak presence was associated with a 53% greater MAS ($P < .001$) and a 60% greater range of the cumulative axial strain ($P < .001$) of the aneurysm sac, while controlling for the type of the agent used. The data showed no significant impact of the presence of endoleak on the range of the cumulative axial shear strain. All cases were included in the generation of these models.

Comparison between Readers

The ICCs of the MAS, range of cumulative axial strain, and range of cumulative axial shear strain were 0.807 (95% CI: 0.754–0.849), 0.842 (95% CI: 0.798–0.877), and 0.874 (95% CI: 0.838–0.902) between segmentations.

DISCUSSION

The goal of the study was to characterize the mechanical properties of the constituents of the aneurysm sacs after endoleak embolization with CH and CH-STS using SUE. CH-STS demonstrated lower strain values than both CH and ILT. There was no significant difference in the ILT

Table 3. Linear Mixed-Effects Model Demonstrating the Effect of the Use of CH-STS (versus CH) on the Elastographic Parameters of the Maximum Axial Strain, Range of Cumulative Axial Strain, and Range of Cumulative Axial Shear Strain of the Embolic Agent Region of Interest

Predictor	Maximum axial strain			Range of cumulative axial strain			Range of cumulative axial shear strain		
	Estimate	95% CI	P value	Estimate	95% CI	P value	Estimate	95% CI	P value
Intercept	0.22%	0.15% to 0.32%	<.001	0.52%	0.37% to 0.73%	<.001	0.65%	0.42% to 0.98%	.042
Use of CH-STS	−66%	−80% to −42%	<.001	−67%	−79% to −47%	<.001	6%	−42% to 96%	.845

Note–The estimate for the predictor CH-STS refers to the percentage change of the outcome parameter when CH-STS is used. Subject was a random effect.
CH = chitosan hydrogel; CH-STS = chitosan hydrogel with sodium tetradecyl sulfate.
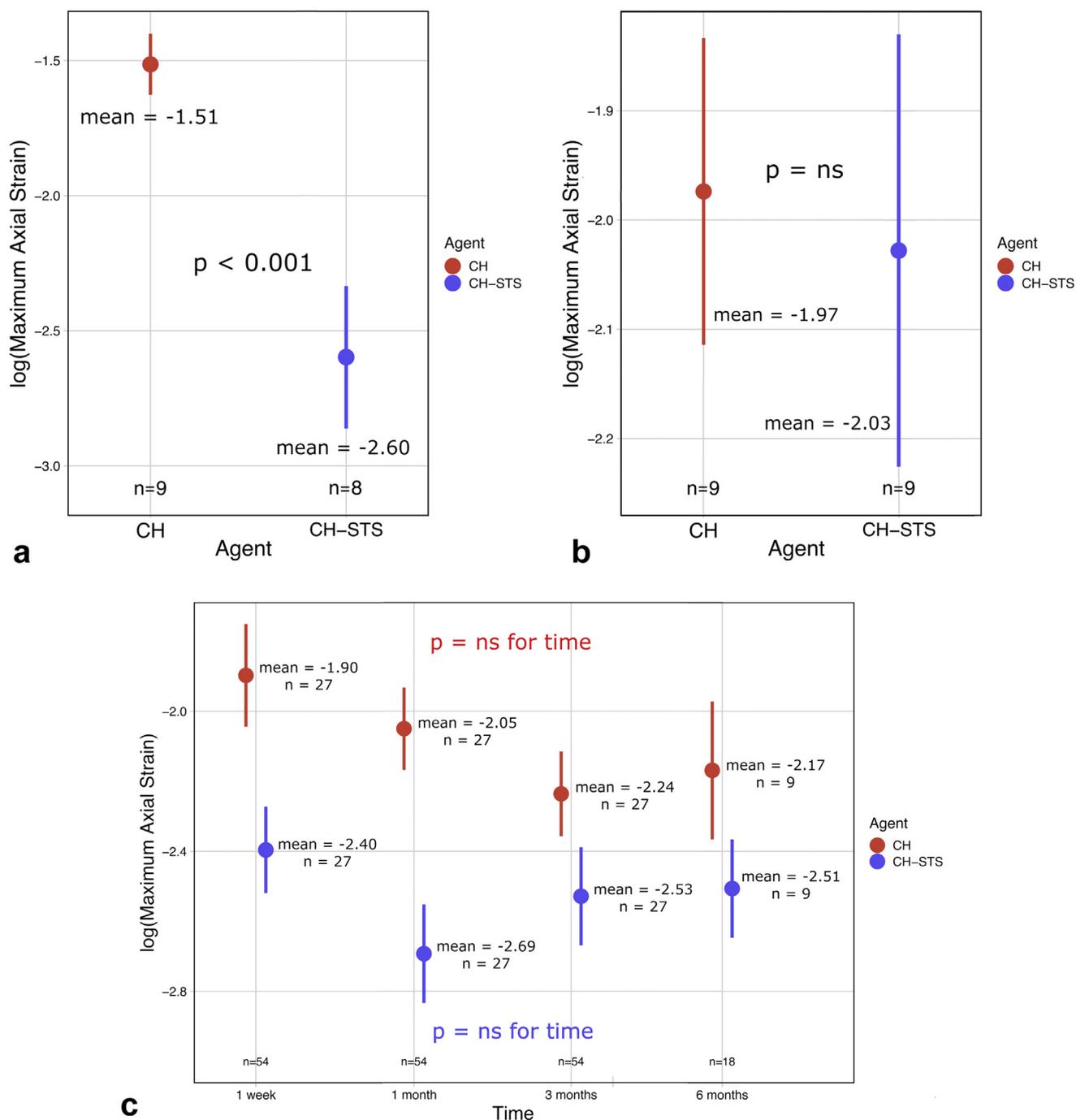
Figure 3. Comparison of the maximum axial strain (MAS) values of the embolic agent, intraluminal thrombus, and aneurysm sac regions of interest (ROIs) after embolization with the chitosan hydrogel with sodium tetradecyl sulfate (CH-STS) versus the chitosan hydrogel (CH) at sacrifice. Means and standard errors of the data points in each group are provided. The outcomes were log transformed to produce better model fits. Statistical analyses were performed using multivariable linear mixed-effects models. **(a)** Comparison of the MAS of the embolic agent ROI after embolization with CH-STS versus CH at sacrifice. CH-STS had a significantly lower MAS than CH ($P < .001$). **(b)** Comparison of the MAS of the intraluminal thrombus ROI after endoleak embolization with CH-STS versus CH at sacrifice. There was no significant difference in the MAS of the intraluminal thrombus after embolization with CH-STS versus CH (P = nonsignificant). **(c)** Comparison of the MAS of the aneurysm sac ROI after endoleak embolization with CH-STS versus CH over time. There was no significant difference in the mechanical properties over time for the aneurysm sac ROI after embolization with CH-STS or CH (P = nonsignificant for time). However, the use of CH-STS was associated with a 29% ($P < .001$) decrease in the MAS of the aneurysm sac compared with the use of CH, even when controlling for the presence of endoleak, in the final model.

Table 4. Maximum Axial Strain, Range of Cumulative Axial Strain, and Range of Cumulative Axial Shear Strain of the Intraluminal Thrombus Region of Interest Stratified by the Type of Embolic Agent Used and the Presence of Endoleak

Embolic agent	Endoleak present	Maximum axial strain (%)	Range of cumulative axial strain (%)	Range of cumulative axial shear strain (%)
CH-STS	Yes (n = 4)	0.185 ± 0.108	0.380 ± 0.192	0.865 ± 0.793
	No (n = 5)	0.126 ± 0.053	0.288 ± 0.164	0.458 ± 0.236
CH	Yes (n = 7)	0.155 ± 0.076	0.366 ± 0.152	0.671 ± 0.419
	No (n = 2)	0.133 ± 0.018	0.284 ± 0.069	0.462 ± 0.411

Note–Values are presented as mean ± standard deviation.
CH = chitosan hydrogel; CH-STS = chitosan hydrogel with sodium tetradecyl sulfate.

mechanical properties between the treatment groups. The aneurysm sacs embolized with CH-STS had lower strain and shear strain values than those embolized with CH; furthermore, the sacs with residual endoleaks had greater

strain values than those without endoleaks. SUE segmentations demonstrated good interrater reliability (15).

The importance of the mechanical properties of an embolic agent reflects 2 principles: occlusivity and wall stress reduction. Agents that are stiffer are better able to resist blood flow, thereby reducing the risk of sac recanalization and expansion (3,4). Stiffer intraluminal content also reduces wall stress, which may reduce the risk of rupture (9,12). The finding that CH-STS deformed significantly less than CH correlates well with in vitro rheometry data, which showed that STS improves the mechanical properties of CHs by increasing chitosan chain aggregation (3,4). This finding, along with the observations that CH-STS deformed less than the ILT, that embolization with CH-STS resulted in fewer residual endoleaks (although not significantly, possibly due to small sample size), and that CH-STS has been found to denude the endothelium and be thrombogenic, all legitimize the use of CH-STS as an embolic agent (4,16). Of note, the finding that endoleak

Table 5. Linear Mixed-Effects Model Demonstrating the Effect of the Use of CH-STS (versus CH) on the Elastographic Parameters of Maximum Axial Strain, Range of Cumulative Axial Strain, and Range of Cumulative Axial Shear Strain of the Intraluminal Thrombus Region of Interest

Predictor	Maximum axial strain			Range of cumulative axial strain			Range of cumulative axial shear		
	Estimate	95% CI	P value	Estimate	95% CI	P value	Estimate	95% CI	P value
Intercept	0.11%	0.07% to 0.19%	<.001	0.26%	0.17% to 0.39%	<.001	−0.34%	0.16% to 0.69%	.003
Use of CH-STS	3%	−32% to 58%	.877	−3%	−28% to 32%	.864	24%	−36% to 141%	.529
Presence of endoleak	30%	−20% to 112%	.292	35%	−7% to 97%	.110	62%	−20% to 228%	.183

Note–The estimates for the nonintercept predictors refer to the percentage change of the outcome when the predictor is present. Subject was a random effect.
CH = chitosan hydrogel; CH-STS = chitosan hydrogel with sodium tetradecyl sulfate.

Table 6. Maximum Axial Strain, Range of Cumulative Axial Strain, and Range of Cumulative Axial Shear Strain of The Aneurysm Sac Region of Interest Stratified by Embolic Agent Used (CH versus CH-STS), Presence of Residual Endoleak, and Time

Maximum axial deformation (%)					
Embolic agent	Presence of endoleak	1 wk	1 mo	3 mo	6 mo
CH-STS	Yes	0.143 ± 0.073 n = 4	0.124 ± 0.098 n = 4	0.151 ± 0.106 n = 4	0.117 ± 0.039 n = 1
	No	0.081 ± 0.037 n = 5	0.061 ± 0.028 n = 5	0.068 ± 0.046 n = 5	0.073 ± 0.023 n = 2
CH	Yes	0.230 ± 0.195 n = 7	0.172 ± 0.083 n = 7	0.122 ± 0.069 n = 7	0.122 ± 0.066 n = 1
	No	0.101 ± 0.053 n = 2	0.081 ± 0.042 n = 2	0.133 ± 0.043 n = 2	0.138 ± 0.087 n = 2

Range of cumulative axial deformation (%)					
Embolic agent	Presence of endoleak	1 wk	1 mo	3 mo	6 mo
CH-STS	Yes	0.335 ± 0.197 n = 4	0.243 ± 0.177 n = 4	0.474 ± 0.541 n = 4	0.276 ± 0.091 n = 1
	No	0.201 ± 0.090 n = 5	0.164 ± 0.092 n = 5	0.169 ± 0.118 n = 5	0.158 ± 0.079 n = 2
CH	Yes	0.558 ± 0.484 n = 7	0.440 ± 0.268 n = 7	0.415 ± 0.419 n = 7	0.247 ± 0.157 n = 1
	No	0.223 ± 0.106 n = 2	0.198 ± 0.133 n = 2	0.323 ± 0.130 n = 2	0.261 ± 0.089 n = 2

Range of cumulative axial shear strain (%)					
Embolic agent	Presence of endoleak	1 wk	1 mo	3 mo	6 mo
CH-STS	Yes	0.583 ± 0.311 n = 4	0.430 ± 0.285 n = 4	0.859 ± 0.853 n = 4	0.258 ± 0.084 n = 1
	No	0.512 ± 0.367 n = 5	0.456 ± 0.277 n = 5	0.458 ± 0.244 n = 5	0.575 ± 0.209 n = 2
CH	Yes	0.900 ± 0.698 n = 7	0.725 ± 0.390 n = 7	0.832 ± 1.114 n = 7	0.463 ± 0.362 n = 1
	No	0.486 ± 0.405 n = 2	0.459 ± 0.270 n = 2	0.527 ± 0.164 n = 2	0.698 ± 0.396 n = 2

Note–Values are presented as mean ± standard deviation. "n" indicates the number of aneurysms (with 3 observations per aneurysm).
CH = chitosan hydrogel; CH-STS = chitosan hydrogel with sodium tetradecyl sulfate.

Table 7. Multivariable Linear Mixed-Effects Model Examining the Effect of Embolization with CH-STS (versus CH) and Presence of Residual Endoleak (versus Absence) on the Elastographic Parameters Maximum Axial Strain, Range of Cumulative Axial Strain, and Range of Cumulative Axial Shear Strain of the Aneurysm Sac Contents

Predictor	Maximum axial strain			Range of cumulative axial strain			Range of cumulative axial shear strain		
	Estimate	95% CI	P value	Estimate	95% CI	P value	Estimate	95% CI	P value
Intercept	0.09%	0.07% to 0.12%	<.001	0.22%	0.17% to −30%	<.001	0.66%	0.47% to 0.92%	.015
Use of CH-STS	−29%	−41% to −14%	<.001	−28%	−40% to −14%	<.001	−27%	−39% to −13%	<.001
Presence of endoleak	53%	21% to 92%	<.001	60%	27% to 101%	<.001	−14%	−31% to 8%	.186

Note–The estimates for the nonintercept predictors refer to the percentage change of the outcome when the predictor is present. Subject was a random effect. CH = chitosan hydrogel; CH-STS = chitosan hydrogel with sodium tetradecyl sulfate.

persistence was not a significant predictor of agent strain suggests that the differences in strain measured between CH-STS and CH reflect actual differences in their intrinsic mechanical properties, rather than being confounded by the additional flow-induced deforming force. This is particularly notable, given the differences in residual endoleaks between the treatment groups (ie, although CH embolization was associated with more residual endoleaks, endoleak presence did not predict CH stain). However, future studies with greater sample sizes would be required to definitively exclude the potentially confounding role of endoleak persistence in this relationship.

ILTs are often found in AAAs and act as a mechanical shield (17). The finding that embolization with CH-STS did not improve the mechanical properties of ILT was not unexpected. Although STS is thrombogenic, it does not necessarily improve the thrombus quality (18,19). Furthermore, given that aneurysm creation was performed 8 weeks before the endovascular repair, some ILTs may have been deposited before treatment (13). The finding that endoleak presence did not significantly impact ILT strain was somewhat unexpected, however, as endoleaks could supply the ILT with antithrombotic substances (decreasing organization) (20). However, given that there was a (nonsignificant) trend for lower ILT strain in the no-endoleak groups and that the presence of endoleak did influence the aneurysm sac strain, the study may have been underpowered to detect this relationship. That said, the literature regarding the elastographic properties of ILTs with residual endoleaks is mixed. One study (21) found that ILTs in patients who developed endoleaks were stiffer than those who did not. Another study (22) found that there was no difference in the mechanical properties of ILT between patients with and without endoleaks. Finally, a third study (23) found decreased thrombus organization in aneurysms with residual endoleak.

The aneurysm sac ROI is a composite of the sac constituents (embolic agent and ILT) and would be a useful parameter to quantify overall aneurysm stability clinically as it is easily segmented. The finding of a lower sac strain in aneurysms embolized with CH-STS was likely driven by the agent's mechanical properties (see above). The finding that the endoleak presence was associated with a greater aneurysm sac strain has 2 possible interpretations: (a) endoleaks provided a second deforming force, which was

better elucidated for this ROI, given the greater number of data points, or (b) because the aneurysm contents were more prone to deform, endoleaks were more likely to form. Regardless, this is a useful finding clinically and—when combined with prior data that demonstrate that SUE can identify endoleaks (7)—further supports the role of SUE in both the characterization of sac mechanical properties and in endoleak detection. This may be particularly useful when permanently radiopaque embolic agents (eg, coils, Onyx) impair endoleak detection on CT or when patients cannot receive intravenous contrast. Interestingly, time was not a clinically significant predictor of sac mechanical properties, suggesting that embolization has an all-or-nothing effect on sac strain, instead of causing progressive depressurization. Alternatively, there may have been 2 counteracting processes: thrombus organization and progressive gel degradation (with replacement by fibrous tissue) (4,24).

The SUE segmentations demonstrated favorable interobserver reliability, with ICCs of >0.8 for all 3 outcomes. This suggests that the strain measurements obtained were reliable and not due to an individual operator error. More globally, the high ICCs also further legitimize the role of SUE in patient follow-up. ICCs of >0.7 are generally considered to be above the cutoff for a test parameter to be considered clinically useful, with ICCs of >0.8 becoming more desirable with further validation (15). Since SUE is an adjunctive technique to Doppler ultrasound, as opposed to one that will replace it, the authors believe that this study further justifies the technique's investigation clinically, with aims at increasing the interobserver reliability to closer to 0.9. Future studies will be required to mitigate the unavoidable sources of variability found in everyday practice.

Shear-wave imaging has been proposed as another technique to characterize the mechanical properties of AAAs after endovascular repair (22). Although quantitative, it is limited by a poor penetration of the acoustic radiation force impulses, hindering the assessment of the posterior aneurysm sac (25). This is less problematic for SUE, as the deformations are generated by the vessel itself. Shear-wave imaging also relies on several assumptions regarding tissue homogeneity and tissue isotropy, which may be inaccurate in the intravascular setting. This may explain why it was unable to reliably distinguish CH, CH-STS, and the ILT in the same model (24).

The present study has a few limitations. Surgically created aneurysms do not recreate the underlying pathophysiology from which AAAs tend to arise. The high-flow type I endoleak model was challenging and resulted in a higher incidence of residual endoleaks after embolization than would be expected clinically. The model also favored the presence of high-flow residual endoleaks after failed embolization, which may have overemphasized the differences in the sac strain between the treatment success and failure groups. Clinically, however, the observation of a high sac strain associated with high-flow endoleaks is more relevant, as these endoleaks are more likely to merit reintervention. SUE is limited because it cannot be used to calculate the absolute values of stiffness (the stress condition is unknown), it is subject to motion artifacts, and it is a 2-step process that requires subsequent processing. Wall stress was not directly measured in this study, which is another parameter to gauge rupture risk. However, wall stress analysis is typically performed with finite element analysis requiring a 3-dimensional geometry (beyond the scope of the study), it uses assumptions of constant wall thickness to calculate stress (not applicable in the present study and potentially not in appropriate in clinical practice), and it would not characterize the agents' mechanical properties (12,26). Finally, this exploratory study is limited in its ability to predict future outcomes (eg, sac expansion, rupture). Regardless, the findings do add to the body of evidence supporting the use of CH-STS in the treatment of endoleaks and reaffirm the literature supporting the role of SUE in the follow-up of endoleaks.

In conclusion, SUE was used to compare the mechanical properties of the aneurysm content after endoleak embolization with the experimental agents CH and CH-STS. CH-STS conferred better mechanical properties to the aneurysm sac content than embolization with a similar nonsclerosing agent. Residual endoleaks, regardless of the agent used, are associated with a greater sac strain, an observation that may offer a more nuanced patient follow-up.

ACKNOWLEDGMENTS

AUTHOR INFORMATION

From Laboratoire clinique du traitement de l'image (L.S., H.A., A.B-G., G.S.), Laboratoire de biomatériaux endovasculaires (S.L., F.Z.), and Laboratoire de biorhéologie et d'ultrasonographie médicale (A.B.-G., M.-H.R.-C., G.C.), Centre de recherche du Centre hospitalier de l'Université de Montréal, Montréal, Québec, Canada; Université de Montréal (L.S., A.B.-G.), Montréal, Québec, Canada; Department of Diagnostic Radiology (L.S.), McGill University, Montréal, Québec, Canada; King Khalid University Hospital (H.A.), Radiology and Medical Imaging Department, Riyadh, Riyadh, Saudi Arabia; Département de génie mécanique (S.L.), École de technologie supérieure, Department of Mechanical Engineering, Montréal, Québec, Canada; Département de chimie, biochimie et physique (A.B.-G.), Université du Québec à Trois-Rivières, Trois-Rivières, Québec, Canada; Department of Radiology (É.T., G.S.), Centre hospitalier de l'Université de Montréal, Montréal, Québec, Canada; and McGill University (S.B.), Montréal, Québec, Canada. Received April 16, 2021; final revision received January 7, 2022; accepted February 1, 2022. Address correspondence to G.S., Laboratoire clinique du traitement de l'image, Centre de recherche du Centre hospitalier de l'Université de Montréal, R11.448-900 St Denis, H2X 0A9, Montréal, Québec, Canada; E-mail: gilles.soulez.med@ssss.gouv.qc.ca

REFERENCES

1. Abularrage CJ, Patel VI, Conrad MF, Schneider EB, Cambria RP, Kwolek CJ. Improved results using Onyx glue for the treatment of persistent type 2 endoleak after endovascular aneurysm repair. J Vasc Surg 2012; 56:630–666.
2. Soulez G, Lerouge S, Darsaut T, Salazkin I, Oliva VL, Raymond J. Role of the endothelial lining in endoleak formation and persistence after endovascular repair of aneurysm. J Vasc Interv Radiol 2008; 19: 1070–1078.
3. Fatimi A, Chabrot P, Berrahmoune S, Coutu JM, Soulez G, Lerouge S. A new injectable radiopaque chitosan-based sclerosing embolizing hydrogel for endovascular therapies. Acta Biomater 2012; 8:2712–2721.
4. Zehtabi F, Dumont-Mackay V, Fatimi A, et al. Chitosan-sodium tetradecyl sulfate hydrogel: characterization and preclinical evaluation of a novel sclerosing embolizing agent for the treatment of endoleaks. Cardiovasc Intervent Radiol 2017; 40:576–584.
5. Maurice RL, Daronat M, Ohayon J, Stoyanova E, Foster FS, Cloutier G. Non-invasive high-frequency vascular ultrasound elastography. Phys Med Biol 2005; 50:1611–1628.
6. Mercure E, Destrempes F, Roy Cardinal MH, et al. A local angle compensation method based on kinematics constraints for non-invasive vascular axial strain computations on human carotid arteries. Comput Med Imaging Graph 2014; 38:123–136.
7. Salloum E, Bertrand-Grenier A, Lerouge S, et al. Endovascular repair of abdominal aortic aneurysm: follow-up with noninvasive vascular elastography in a canine model. Radiology 2016; 279:410–419.
8. Fromageau J, Lerouge S, Maurice RL, Soulez G, Cloutier G. Noninvasive vascular ultrasound elastography applied to the characterization of experimental aneurysms and follow-up after endovascular repair. Phys Med Biol 2008; 53:6475–6490.
9. Speelman L, Schurink GW, Bosboom EM, et al. The mechanical role of thrombus on the growth rate of an abdominal aortic aneurysm. J Vasc Surg 2010; 51:19–26.
10. Nguyen VL, Leiner T, Hellenthal FA, et al. Abdominal aortic aneurysms with high thrombus signal intensity on magnetic resonance imaging are associated with high growth rate. Eur J Vasc Endovasc Surg 2014; 48: 676–684.
11. Cornelissen SA, Verhagen HJ, van Herwaarden JA, Vonken EJ, Moll FL, Bartels LW. Lack of thrombus organization in nonshrinking aneurysms years after endovascular abdominal aortic aneurysm repair. J Vasc Surg 2012; 56:938–942.
12. Khosla S, Morris DR, Moxon JV, Walker PJ, Gasser TC, Golledge J. Meta-analysis of peak wall stress in ruptured, symptomatic and intact abdominal aortic aneurysms. Br J Surg 2014; 101:1350–1357; discussion 1357.
13. Soulez G, Lerouge S, Salazkin I, Darsaut T, Oliva VL, Raymond J. Type I and collateral flow in experimental aneurysm models treated with stent-grafts. J Vasc Interv Radiol 2007; 18:265–272.
14. Destrempes F, Meunier J, Giroux MF, Soulez G, Cloutier G. Segmentation of plaques in sequences of ultrasonic B-mode images of carotid arteries based on motion estimation and a Bayesian model. IEEE Trans Biomed Eng 2011; 58.
15. Portney LG, Gross G. Measurement revisited: reliability and validity statistics. Foundations of clinical research: applications to evidence-based practice. 4th ed. Philadelphia (PA): F.A. Davis; 2020: 486–508.

16. Fatimi A, Zehtabi F, Lerouge S. Optimization and characterization of injectable chitosan-iodixanol-based hydrogels for the embolization of blood vessels. J Biomed Mater Res B Appl Biomater 2016; 104: 1551–1562.

17. Wang DH, Makaroun MS, Webster MW, Vorp DA. Effect of intraluminal thrombus on wall stress in patient-specific models of abdominal aortic aneurysm. J Vasc Surg 2002; 36:598–604.

18. Albanese G, Kondo KL. Pharmacology of sclerotherapy. Semin Intervent Radiol 2010; 27:391–399.

19. Parsi K, Exner T, Low J, Fung Ma DD, Joseph JE. In vitro effects of detergent sclerosants on clot formation and fibrinolysis. Eur J Vasc Endovasc Surg 2011; 41:267–277.

20. Ajjan RA, Standeven KF, Khanbhai M, et al. Effects of aspirin on clot structure and fibrinolysis using a novel in vitro cellular system. Arterioscler Thromb Vasc Biol 2009; 29:712–717.

21. Bando Y, Kitase M, Shimohira M, et al. 2D-shear wave elastography in the prediction of type II endoleaks after endovascular aneurysm repair. Minim Invasive Ther Allied Technol 2021; 30:21–26.

22. Voizard N, Bertrand-Grenier A, Alturkistani H, et al. Feasibility of shear wave sonoelastography to detect endoleak and evaluate thrombus organization after endovascular repair of abdominal aortic aneurysm. Eur Radiol 2020; 30:3879–3889.

23. Bertrand-Grenier A, Lerouge S, Tang A, et al. Abdominal aortic aneurysm follow-up by shear wave elasticity imaging after endovascular repair in a canine model. Eur Radiol 2017; 27:2161–2169.

24. Bertrand-Grenier A, Zehtabi F, Lerouge S, et al. Shear wave elasticity imaging for residual endoleak and thrombus characterisation after endoleak embolisation following endovascular aneurysm repair: a canine animal study. Eur Radiol Exp 2018; 2:28.

25. Carlsen JF, Pedersen MR, Ewertsen C, et al. A comparative study of strain and shear-wave elastography in an elasticity phantom. AJR Am J Roentgenol 2015; 204:W236–W242.

26. van Disseldorp EMJ, Petterson NJ, van de Vosse FN, van Sambeek MRHM, Lopata RGP. Quantification of aortic stiffness and wall stress in healthy volunteers and abdominal aortic aneurysm patients using time-resolved 3D ultrasound: a comparison study. Eur Heart J Cardiovasc Imaging 2019; 20:185–191.

APPENDIX A. MATERIALS AND METHODS

Surgical Creation of Aneurysms

Aneurysms were created surgically under general anesthesia using sterile conditions by a vascular surgeon with >20 years' experience (I.S.). The lateral neck of each dog was incised to harvest an external jugular vein, which was placed in heparinized solution. A low-midline laparotomy was performed. The overlying small bowel was retracted, and the common iliac arteries and sacroiliac trunks were exposed and mobilized. For each iliac artery, the proximal and distal aspects of the vessel were cross-clamped, and a longitudinal arteriotomy was performed. Subsequently, a sacroiliac trunk branch was isolated, transected, and anastomosed to the arteriotomy site. A patch was measured and cut from the harvested external jugular vein, placed over the arteriotomy site with stay sutures, and then sutured in place with 7.0 Prolene. The artery was reperfused. The procedure was repeated on the contralateral common iliac artery. The bowel was repositioned, and the peritoneal incisions were closed. Using this technique, aneurysms with a diameter of 20–25 mm (normal common iliac artery diameter of approximately 5 mm) and a length of 30–35 mm were created (1).

Endovascular Aneurysm Repair, Endoleak Creation, and Embolization

Endovascular aneurysm repair (EVAR), endoleak creation, and embolization were performed 8 weeks after aneurysm creation by an interventional radiologist with 30 years' experience (G.S.). First, 4-F sheaths were inserted into the common femoral arteries bilaterally, and a 7-F sheath was inserted into the left carotid artery. One aneurysm was selected for EVAR, endoleak creation, and embolization, all of which would then be performed on the contralateral side. The tip of a 4-F Glidecath (Terumo, Tokyo, Japan) was placed into the targeted aneurysm via the contralateral puncture (up-and-over) to prepare for embolization. A 3.5-mm balloon (Powerflex; Cordis, Warren, New Jersey) was placed in the proximal common iliac artery of the targeted aneurysm using the ipsilateral femoral access. A 7-mm or 8-mm × 59-mm balloon-expandable stent (sized based on the diameter of the normal artery) (iCAST; Atrium, Hudson, New York) was then placed into the aneurysm sac via the carotid access. EVAR was performed, creating proximal and distal landing zones of approximately 10 mm. Type Ia endoleaks were created by withdrawing the uninflated balloon into the proximal landing zone and inflating it to deform the stent. The 3.5-mm balloon was then deflated and carefully removed. The stent balloon was retracted into the proximal common iliac artery, and the endoleak presence was confirmed with angiography (Koordinat 3D II; Siemens, Erlangen, Germany). The stent balloon was then reinflated, and the embolic agent was deployed into the endoleak using the Glidecath. The embolization endpoint was nidal occlusion; approximately 5 mL of gel was used. The procedure was then repeated on the contralateral side using the other agent.

Preparation of Chitosan Hydrogel and Chitosan Hydrogel with Sodium Tetradecyl Sulfate

Chitosan hydrogel (CH) and CH with sodium tetradecyl sulfate (CH-STS) were prepared using a previously published methodology, which will be summarized (2,3). To prepare CH-STS, chitosan powder (Marinard Biotech, Rivière-au-Renard, Canada) was dissolved in a solution of Visipaque 320 (GE Healthcare, Rahway, New Jersey), hydrochloric acid (0.1 M), and deionized water. The solution was stirred for 24 hours and subsequently placed in an autoclave for sterilization. Another solution was prepared of β-glycerophosphate disodium hydrate (BGP) (Sigma Aldrich, Oakville, Canada) and sodium tetradecyl sulfate (STS) (Sigma Aldrich). This was sterilized using a 0.2-μm filter. Prior to the procedure, the solutions were mixed with two 5-mL syringes and a luer lock connector. The volume ratio was 3:2 of the chitosan and Visipaque solution to the BGP and STS solution. CH-STS solution was composed of the final following concentrations: chitosan 2% weight/volume; STS 3% weight/volume; Visipaque 320 30% volume/volume; and BGP 12% weight/volume. CH solution was made in a similar fashion, but it did not include STS; a final concentration of BGP of 20% weight/volume was used instead.

Blinding and Randomization of Embolization

In each animal, 1 aneurysm was randomly selected to be embolized with CH-STS, and the other, with CH. This was performed to avoid operator bias with respect to technical preference for working on a particular side of the subject while using a given agent (ie, subject left versus right) and to avoid bias for treating more challenging/simpler aneurysm with a given agent. On the day of the embolization procedure, the embolic agents—prepared in advance by a biomedical engineer graduate student (F.Z.)—were randomly coded as "1" or "2," placed in labeled envelopes, and then provided to the interventional radiologist for embolization. One aneurysm was then embolized with "1," whereas the other was embolized with "2." Therefore, the interventional radiologist (G.S.) was blinded to the type of the used agent to treat a given endoleak. The side embolized by each coded agent was recorded. The agents' identities were decoded at the end of the experiment.

Imaging Parameters

B-mode and Doppler images were acquired using the SuperLinear 256 element SL15-4 7.5 MHz transducer

(Aixplorer, Aix-en-Provence, France). Doppler ultrasound parameters were set to the following: scale, 10 cm/s; smoothing, 0; wall filter, low; high-definition frame rate, middle; and steer angle, 0°, 60° right anterior oblique, and 60° left anterior oblique. Radiofrequency cines for strain ultrasound elastography were acquired with Sonix Touch 128-element L14-5/38 10-MHz transducer (Ultrasonix Medical Corporation, Vancouver, Canada). The probe had a frame rate of 25 Hz and a bandwidth of 60%. Acquisitions were sampled at 40 MHz for 4 seconds. Computed tomography studies were obtained in the arterial and venous phases with the SOMATOM Sensation 64 (Siemens Medical, Forcheim, Germany) using 60 mL of Omnipaque 300 (GE Healthcare, Mississauga, Canada) injected at 4 mL/s. The acquisition parameters were as follows: prospective gating with 10 image/cycle reconstructions during diastole; voltage, 120 kVp; current, 724 mA; pitch, 0.2 mm; and collimation, 0.6 mm.

Tissue Preparation

Animals were sacrificed using intravenous pentobarbital sodium (Euthanyl Forte, 108 mg/kg; Bimeda-MTC Animal Health, Cambridge, Canada). Aneurysms were harvested en bloc and fixed in buffered formalin. Serial axial macroscopic sections were obtained using a cutting-grinding system (EXAKT, Norderstedt, Germany). These were photographed for a macroscopic analysis. Representative histological slides were also produced to correlate the macroscopic and microscopic findings. These slides were prepared by removing the stent graft, embedding the slides in paraffin, and staining with hematoxylin phloxine saffron. Macroscopic and histologic analyses were supervised by a biomedical engineer with >20 years' experience in biomaterial research (S.L.).

Computation of Strain

Each region of interest (ROI) was segmented on an initial frame by the reader. Beginning with this reference frame, an algorithm was employed to track and refine the ROI on the subsequent frames based on the ROI motion field, statistics of the radiofrequency echo envelope intensity levels, and the prior geometry. The strain components were then determined by tracking the movement and morphologic changes of the ultrasonic speckles using a Lagrangian speckle model estimator. In the first step, the translation motion of the speckles was estimated using a cross-correlation method. In the second step, the strain components (characterized by the changes in morphology of the speckles) were computed by solving an extended version of the optical flow equation (4).

Statistical Analysis

Linear mixed-effects models were primarily used for statistical analysis for the following reasons: (*a*) they are able to tolerate unbalanced data, (*b*) they avoid eliminating all the data from a subject when an observation is missing, and (*c*) they are able to better account for repeated measurements on the same subject (5). For the agent ROI model, the agent used was the primary factor in the final model. For the intraluminal thrombus ROI model, the agent used and the presence of endoleak were the primary factors in the final model. For the aneurysm sac ROI model, the type of the agent and the presence of endoleak were the primary factors for the final model.

REFERENCES

1. Soulez G, Lerouge S, Salazkin I, Darsaut T, Oliva VL, Raymond J. Type I and collateral flow in experimental aneurysm models treated with stent-grafts. J Vasc Interv Radiol 2007; 18:265–272.
2. Fatimi A, Chabrot P, Berrahmoune S, Coutu JM, Soulez G, Lerouge S. A new injectable radiopaque chitosan-based sclerosing embolizing hydrogel for endovascular therapies. Acta Biomater 2012; 8:2712–2721.
3. Zehtabi F, Dumont-Mackay V, Fatimi A, et al. Chitosan-sodium tetradecyl sulfate hydrogel: characterization and preclinical evaluation of a novel sclerosing embolizing agent for the treatment of endoleaks. Cardiovasc Intervent Radiol 2017; 40:576–584.
4. Maurice RL, Daronat M, Ohayon J, Stoyanova E, Foster FS, Cloutier G. Non-invasive high-frequency vascular ultrasound elastography. Phys Med Biol 2005; 50:1611–1628.
5. McCulloch CE. Repeated measures ANOVA, R.I.P.? Chance 2005; 18:29–33.
6. Salloum E, Bertrand-Grenier A, Lerouge S, et al. Endovascular repair of abdominal aortic aneurysm: follow-up with noninvasive vascular elastography in a canine model. Radiology 2016; 279:410–419.
7. Fromageau J, Lerouge S, Maurice RL, Soulez G, Cloutier G. Noninvasive vascular ultrasound elastography applied to the characterization of experimental aneurysms and follow-up after endovascular repair. Phys Med Biol 2008; 53:6475–6490.

Table E1. B-Mode, Doppler Ultrasound, Computed Tomography, and Histopathologic Appearance of the ROIs to be Characterized by Strain Ultrasound Elastography (Agent, Thrombus, and Aneurysm Sac), as Well as Other ROIs Used to Help Delineate them (Endoleak and Stent Graft)

Region	Ultrasound	Computed tomography	Macroscopy	Microscopy
Embolic agent (CH or CH-STS)*	Hyperechoic to the thrombus	Indistinguishable from the thrombus[†]	Yellow-brown, homogenous, friable material	Red/purple material lacking cellular content or tissular organization
Thrombus*	Hypoechoic to the embolic agent	Indistinguishable from the embolic agent[†]	Organized: dense yellow, organized tissue Fresh: dark blue, unorganized tissue	Organized: layered network of fibrin. Fresh: free, unstructured erythrocytes
Aneurysm sac[‡]	Entire aneurysm content minus the endoleak and stent graft	Entire aneurysm content minus endoleak and stent graft	Entire aneurysm content minus the endoleak and stent graft	Entire aneurysm content minus the endoleak and stent graft
Endoleak[§]	Mobile echoes on B-mode cine. Doppler signal indicating flow on Doppler imaging	Contrast enhancement within the aneurysm but outside the stent graft	Defect within the aneurysm sac	Defect within the aneurysm sac
Stent graft	Hyperechoic ring	Hyperdense ring	Self-evident	Removed for histologic processing

B-mode = brightness mode; CH = chitosan hydrogel; CH-STS = chitosan hydrogel with sodium tetradecyl sulfate; ROI = region of interest.

*The agent and the thrombus were measured at the most representative level per aneurysm at sacrifice.

†CH and CH-STS contain iodixanol but are only temporarily radiopaque.

‡The aneurysm sac's mechanical properties represent overall sac stability. To account for the heterogeneity of the composition of the aneurysm sac, the mechanical properties for 3 levels of the sac (proximal, middle, and distal) were measured.

§Endoleaks were not assessed as an ROI using elastography because they had already been characterized as regions of high strain caused by the heterogeneous effects of signal decorrelation due to slow blood flow and the presence of immature thrombus (6,7).